Utrecht University and ETH Zürich

Bachelor Thesis

GEO3-1324H

The Activity of Basal Stick-Slip Clusters on Rhonegletscher, Switzerland

Author
G.W. Janzing
5634911

Supervisors
Dr. W.W. Immerzeel
Prof. Dr. F. Walter

November 24, 2018

Abstract

Basal stick-slip motion of glaciers has been detected and studied extensively on Antarctic glaciers. It has been shown to represent an important aspect of the dynamics of some specific ice streams. However, stick-slip motion beneath alpine glaciers has had much less scientific attention. This thesis presents an analysis of data spanning almost a year from three seismic stations, which have been placed on Rhonegletscher in the Swiss Alps. Microseismic stick-slip events show clustering at specific locations and two of these clusters were studied in more detail. Their activity was compared to environmental parameters such as solar radiation, air temperature, discharge (as a proxy for melt) and precipitation. It was found that the two clusters show differences in behaviour. One cluster displays strong diurnal variations, which correlate with the environmental parameters (except for precipitation). This suggests that its activity is strongly influenced by meltwater. The other cluster seems unaffected. Furthermore, the latter cluster displays a strong relation between amplitude and interevent times, suggesting a relatively continuous accumulation of stress through time. The first cluster does not show this behaviour. Finally, the interaction of both clusters is studied. It is found that the emitted seismic energy per time of one cluster seems to show opposite behaviour compared to the other. This could indicate that the clusters tap from the same energy reservoir. No evidence for direct triggering of events between clusters could be found, although there are indications for some influence on a time scale of minutes.

Contents

Preface

This thesis was written after a fieldwork of the Labratory of Hydraulics, Hydrology and Glaciology (VAW) of the ETH Zürich in the summer of 2018.

It is important to make clear which parts of the analyses were done by others and which by myself. The spectral detection algorithm was written and run by Dominik Gräff, as was the localisation algorithm. He also created the weighted stacks used for the correlations. The correlation, amplitude and stacking codes were written by Lizzy Clyne, but were adapted and used by me. I took care myself of the further analyses and plotting.

First and foremost, I want to thank Dominik Gräff, whose project I was working on, for his support in- and outside the field. He was always prepared to help me with the analysis of the data during our skype sessions. Furthermore, I want to thank Lizzy Clyne, for her energy and her enthousiasm during the fieldwork, for writing most of the python codes I used for this thesis and especially for her help when I got stuck on them. I further want to thank Sebastian, Andreas, Katalin, Michi, and all staff of VAW that visited us during the field campaign for the memorable days in the field and nights in Hotel Tiefenbach. I also want to thank Hanneke Paulssen from Utrecht University, who suggested some useful ways to look at my data.

Finally, I want to specially thank both Dr. Walter Immerzeel for supervising me during the project and for his support in Utrecht, and Prof. Dr. Fabian Walter for giving me the opportunity to do this field work in the first place and for his advice in the field.

1 Introduction

The study of ice dynamics is critical for understanding the behaviour of glaciers, especially during climate change. In recent years, glaciers have been observed to both accelerate (e.g. Rignot and Kanagaratnam (2006); Scambos et al. (2004)) and slow down (e.g. Neckel et al. (2017)). These changes in glacier dynamics can have consequences worldwide: the exact future rate of sea level rise, for instance, is dependent on changes in glacier motion (Rignot and Kanagaratnam, 2006) and is influenced by processes such as Marine Ice Sheet Instability (MISI), for which the dependence of sliding on friction is a major uncertainty for prediction (Ritz et al., 2015).

There are three basic mechanisms of glacier motion (Cuffey and Paterson, 2010). The first is plastic internal ice deformation (also called creep). Materials can react on the increase of stress in different ways. If the deformation, or strain, is proportional to the applied stress and it is reversible, this behaviour is called elastic. For other materials, not the deformation itself but the rate of deformation is proportional to the stress. This is for example the case with fluids like water and this type of behaviour is called Newtonian viscous. When a material displays perfect plasticity, it does not deform until a specific yield stress is reached. The stress can not exceed this critical value, but the deformation rate can have any value. The creep of ice is an intermediate form between Newtonian viscous behaviour and perfect plasticity (Cuffey and Paterson, 2010).

The other two mechanisms for glacier motion concern the ice-bed interaction. These are deformation of the bed and basal sliding. If the bed beneath a glacier is deformable, which is often the case when there is a till layer, it is called a soft bed. Research has shown that when this is present, internal shear within the bed can account for a large part of the motion of the glacier, especially when the till is water saturated (Cuffey and Paterson, 2010). For basal sliding on a hard substrate, it was originally thought that there were two main mechanisms for glaciers pass obstacles on the bed. The first is called regelation (Weertman, 1957). When the ice hits a bump on the bed, the upstream part will experience a higher pressure than the downstream part. At the upstream part, the pressure melting point is thus lower and the ice around it will start to melt. This meltwater flows around the bump to the lower pressure zone, which has a higher melting point. Therefore, the water freezes again. The released heat is then transported through the obstacle and will cause the ice upstream to melt further. The consequence is that the glacier "flows" around the bump. A second mechanism for basal sliding is called enhanced creep (Weertman, 1957). The presence of an obstacle in the ice flow will increase the stress. By viscous deformation, the ice will compress and stress which will cause it to pass the obstacle. Important assumptions underlying these sliding theories were the idea that the bed rock is not deformable and the existence of a thin layer of water separating ice and bed rock, so no tangential stress could exist (Cuffey and Paterson, 2010; Weertman, 1957).

However, observations of the ice at the bottom of temperate glaciers showed that the interface between ice and bedrock is often not a sharp line. Rather, it is gradual and the ice at the bottom is filled with debris (Cuffey and Paterson, 2010). This contradicted one of the initial assumptions in basal sliding theory, namely the lack of tangential stress at the ice-bed interface.
The discovery of stick-slip motion at the base of glacier proved again that this assumption was false. *Stick-slip behaviour* occurs because of friction on an interface and can be illustrated by a block on a flat surface (Shearer, 2009). The idea is the static friction between the block and the surface is larger than the dynamic friction. When the stress on the block becomes large enough to overcome the static friction, the block will move. However, the stress will reduce. The movement continues until the dynamic friction becomes larger than the stress. The resulting

behaviour is characterised by short phases of rapid movement, followed by quiet phases in which the block rests.

On Whillans Ice Stream in Antarctica, it was discovered that large scale stick-slip activity is an important mechanism for the motion of ice streams (Bindschadler et al., 2003). It was shown that close to the grounding line at a relatively flat region, basal motion occurred in short outbursts of 10 to 30 minutes in which the ice reaches velocities of about 1 meter per hour. This is 30 times faster than the velocity of the smoothly moving Whillans Ice Stream upstream of the ice plain. These short events are separated by quiet periods of 6-18 hours. The size of the moved ice is in the order of 200 km x 100 km with a thickness of 600 m (Wiens et al., 2008).

Stick-slip events on the ice stream also transmit seismic waves (Wiens et al., 2008). These are vibrations that propagate because of the elastic behaviour of the ice. There are two basic types of seismic waves that can originate from a seismic source (Doyle, 1995). When the motion of the vibration is parallel to the travel direction, the wave is characterised by compression and dilation and is called a P-wave (primary), since these waves are the fastest and are the first to arrive at a measuring station (see figure 1). The other basic type of wave is the S-wave (secondary). This is a shear wave, which means that the movement is perpendicular to the way of travelling. Both P- and S-waves can travel through solid bodies and are therefore called body waves. When these waves reach a surface or interface, their interactions can travel together as surface waves of which the two main types are Rayleigh waves and Love waves. In general, these surface waves are characterised by a large amplitude and a lower frequency.

Seismic events caused by glacier motion are called *icequakes*. From the seismic recordings, different sources can be distinguished. Seismic waves of surface events at glaciers, such as crevasse openings are dominated by Rayleigh waves. However, for deep events, surface waves are almost absent and the recorded seismograms are dominated by P- and S-waves (Walter et al., 2009).

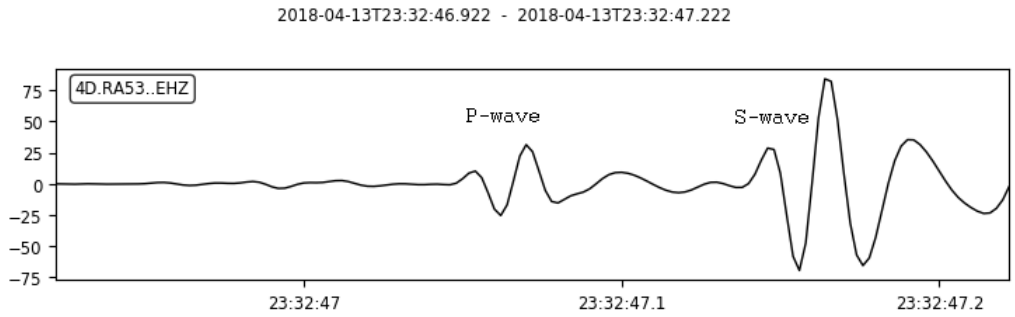

Figure 1: An example of a recorded detection of a basal event by the vertical channel (EHZ) of RA53. P- and S-wave are indicated. The recording filtered with a bandpass between 10 and 120 Hz. Time in UTC.

The shape of a recorded seismic wave is determined by a few factors. The time between the arrival of different types of waves is a function of distance. P-waves travel faster than S-waves (see table 1; see figure 1) and the difference in their arrival times can be used to locate the seismic source (Doyle, 1995). The polarities of the seismogram is determined by the direction of movement. When the P-wave is compressional, this is registered as a positive peak. A tensile movement is seen as negative. When the movement of the seismic source is towards the recording station, the first arriving peak is compressional. In the case of a crack opening, for example, the first peak of the P-waves is positive in all directions. For the closing of a crack, the opposite

Wavetype	Velocity
P-wave	3600-3900 ms^{-1}
S-wave	1700-1950 ms^{-1}

Table 1: Seismic wave velocities in ice (Roethlisberger (1972) as cited in Podolskiy and Walter (2016)).

is true. Only for strike-slip motion, both polarities have to be present, since in the direction of movement the first phase is compressional, but in the opposite direction it is extensional. Finally, the amplitude of a seismic wave is a function of the amount of energy that is released.

It has been shown that the identical locations between the ice and the bed remain sources of stick-slip activity for longer time periods (Helmstetter et al., 2015; Wiens et al., 2008). In classical earthquake seismology, these points are called *asperities*, which are strong points along a fault (Doyle, 1995).

At these locations with higher friction, stress can accumulate during the phases when no slip takes place, until a certain yield stress is reached. Then it slips, which produces a characteristic seismic event. Multiple events with similar waveforms (although they can still have different amplitudes) are often called *clusters* and suggest an isolated and repeating source (Helmstetter et al., 2015).

Although it is clear that for Antarctic ice streams stick-slip behaviour is an important part for their dynamics, this is not settled for other glaciers world wide (Podolskiy and Walter, 2016). Multiple studies at Alpine glaciers have not been able to find seismic activity from basal stick-slip events (Moore et al., 2013; Pomeroy et al., 2013). Laboratory experiments have shown that ice at pressure melting point, which is the case for most alpine glaciers, can only exhibit stable sliding, whereas stick-slip behaviour was reserved for subfreezing ice, which might explain the lack of seismic activity (Zoet et al., 2013). Still, stick-slip events have reportedly been detected for alpine glaciers (e.g. Allstadt and Malone (2014); Thelen et al. (2013)). At Glacier d'Argentière in the French Alps, specific clusters have been observed, which seem to represent stick-slip motion (Helmstetter et al., 2015). However, no mixed polarities could be observed, since only one seismic station was installed. Furthermore, this activity is of a completely different scale than those of the Antarctic ice streams: the slip was estimated to be between 1 μm and 4 mm and durations of about 0.1 s. This is called *microseismicity*.

Laboratory experiments have tried to investigate the physical controls on stick-slip behaviour of glaciers (Zoet et al., 2013). Both a higher debris content of the ice and a higher velocity seemed to favour unstable sliding. The idea is that these conditions will both produce frictional heat with acceleration and therefore a large quantity of meltwater. This water lubricates the contacts between glacier and the bed. The quiet periods can then be caused by a refreezing of the water. Also in the field the controls were studied. It is suggested that seismic activity at the bed is more frequent when no or little deformable sediment is present, in which case more basal sliding occurs (Smith, 2006). Basal seismicity has further been correlated with diurnal subglacial water pressure variations (Walter et al., 2008). When the water pressure is low or decreasing, seismicity increased. However, in this research no mixed polarities were found, so these were probably no stick-slip events. Glacial seismicity can also be initiated by external forces. Bindschadler et al. (2003), for example, found that the stick-slip activity on Whillans Ice Stream correlated with tidal oscillations.

As the exact mechanism behind stick-slip activity for temperate ice remains an open question, more study of the seismic activity on temperate mountain glaciers is necessary. By studying the stick-slip movement of glaciers, the importance of this type of behaviour can be analysed and previous sliding theories might have to be updated or changed (Podolskiy and Walter, 2016).

This thesis studies the behaviour of two stick-slip asperities on the temperate Rhonegletscher for the period from 30-09-2017 until 22-08-2018. This is an observational study which will investigate the controls on their frequency, amplitude and the relation between the activity of the two clusters. Based on the presented literature, it is hypothesised that the availability of meltwater will change basal water pressures and therefore stresses beneath the glacier and will thus favor stick-slip behaviour. Furthermore, it is expected that longer interevent times will lead to more stress accumulation and thus larger amplitudes.

2 Methods

2.1 Study Site

Rhonegletscher is a temperate valley glacier located in the eastern part of the canton of Valais in Switzerland. It is elevated roughly between 2200 m and 3600 m above sea level and is generally north-south oriented (see figure 2) (Gabbi et al., 2014). In 2012, this glacier had a size of 15.8 km^2 and a volume of 1.78 km^3 (Huss and Farinotti, 2012). The maximum thickness in 2009 was 345 meters, with a median thickness of 130 meter (Farinotti et al., 2009).

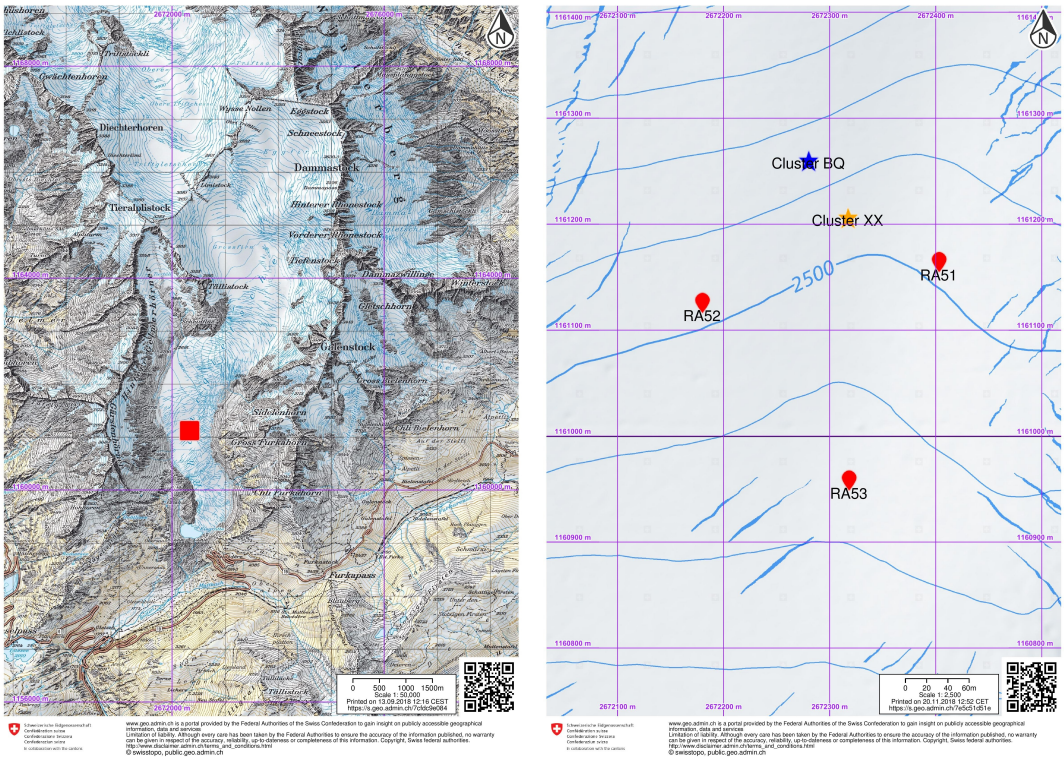

Figure 2: Location of the Rhonegletscher and the three seismic stations which were used in this study on it on 31-07-2018 (note that the seismic stations move with the glacier). The depicted stations in red were located there starting from the end of September 2017 until the end of the study period. In orange and blue are the two stick-slip clusters which were studied in this thesis. Source: swisstopo.

Rhonegletscher has retreated significantly since the Little Ice Age, when its tongue still reached the village of Gletsch. Between 1879 and 2016, it retreated 1.4 km (Glaciological Reports, 2017). For the period of 1980-2010, it was found that the temporally homogenized geodetic mass balance of Rhonegletscher was -0.6 to -0.7 meter w.e.yr^{-}1 (Fischer et al., 2015). Modeling studies have predicted that the glacier will decrease drastically in size in the 21st century and might even completely disappear (Jouvet et al., 2009; Wallinga and Van De Wal, 1998).

Since 2005, a proglacial lake has appeared at the glacier tongue. This has led to a significant increase in the flow velocity at the tongue due to an increase in basal sliding (Sugiyama et al., 2011). On average, the flow velocity in the lower part of the glacier is of the order of 10^1 m/yr (Tsutaki et al., 2011).

The bedrock has only been studied at particular places. This shows that the bed is heterogenous. Some places are underlain by subglacial sediments (till), whereas at other places the hard bedrock is not covered (Sugiyama et al., 2008).

The closest weather station to the Rhonegletscher is the station at Grimsel Hospiz at an elevation of 1980 meter. During the ablation period (April to October) of 2007 until 2012, it was found that the average temperature on the Rhonegletscher was 4.4 degrees Celsius (Gabbi et al., 2014). Furthermore, 503 mm snow fell on average during this ablation period, whereas 6.8 meters w.e. melted.

There are multiple reasons for choosing this particular glacier as our study site. One of the reasons is that it is relatively easily accessible, which is very important since a large quantity of equipment had to be transported during this project. Furthermore, Rhonegletscher has a long history of being studied (at least since the late 19th century: Glaciological Reports (2017); Mercanton et al. (1916)) and therefore there is plenty of data available. Also previous cryoseismological research has been conducted at Rhonegletscher (Dalban Canassy et al., 2016). Therefore, it is known that seismic activity does occur on this glacier.

The investigated part of the glacier lies in the ablation zone and is elevated approximately between 2450 and 2550 meters above sea level, which was chosen because of its relative flatness and the lack of crevasses. At this location, it was determined that the thickness was about 190 meters by means of hot water drilling.

2.2 Data Acquisition in the Field

End of September 2017, three seismic stations were installed in the research area (stations RA51, RA52 and RA53) (see figures 2 and 3). These stations were each equipped with a borehole seismometer of the type Lennartz 3D 1s BH with 1s eigenperiod (also used by Dalban Canassy et al. (2016)), which were installed in the ice at a depth of about four meters (see figure 5).

The borehole seismometers measured the ground velocity caused by seismic vibrations in three directions: two horizontal (named EH2 and EH3: set in a random direction perpendicular to each other) and one vertical (named EHZ). Since EHZ is always oriented in the same way and the seismic waves come from the glacier bed, the polarity of the arriving waves measured by this component shows if the wave is compressional or extensional. For the horizontal components this depends on their directions compared to the seismic source. Since they are set at random, these components are not taken into account when determining if a cluster represents a stick-slip event or not. The seismometers were linked to a pelicase which contained a digitiser (see figure 4). The digitisers of stations RA51 and RA52 were of the type Nanometrics Taurus (also used by Dalban Canassy et al. (2016)). RA53 had a Nanometrics Centaur digitiser. All stations had a sampling rate of 500 Hz. Together, the digitisers and the sensor led for stations RA51 and RA52 to a sensitivity of 4.0e8 cnt/(m/s) and for station RA53 to 6.4e8 cnt/(m/s). The data was stored on an SD-card. It is important that the timing of the recordings is accurate. Therefore, the clocks of the stations were synchronised with the time from satellites by means of a GPS-antenna. Power to the digitisers was provided by both a battery and a solar panel connected to the pelicase.

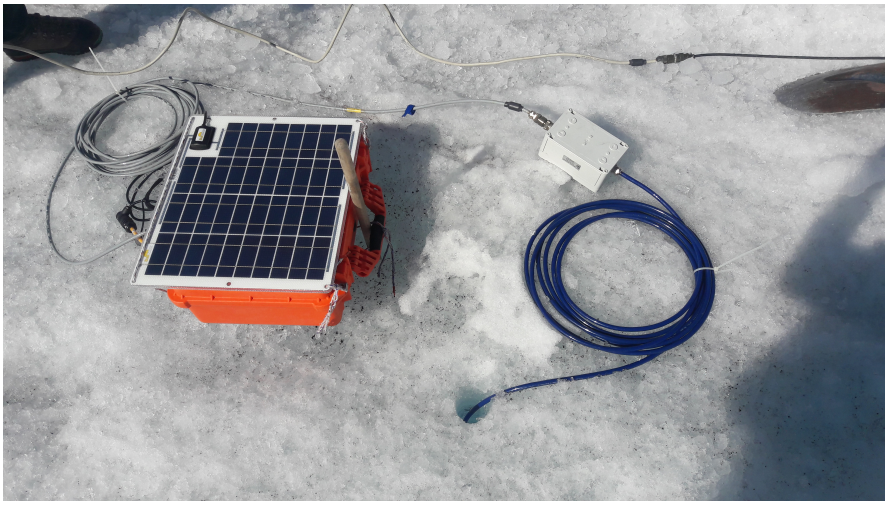

Figure 3: An example of the installed seismic stations. The solar panel on the orange pelicase provides part of the energy. The blue cable is attached to the sensor, which is 2 meters below the surface.

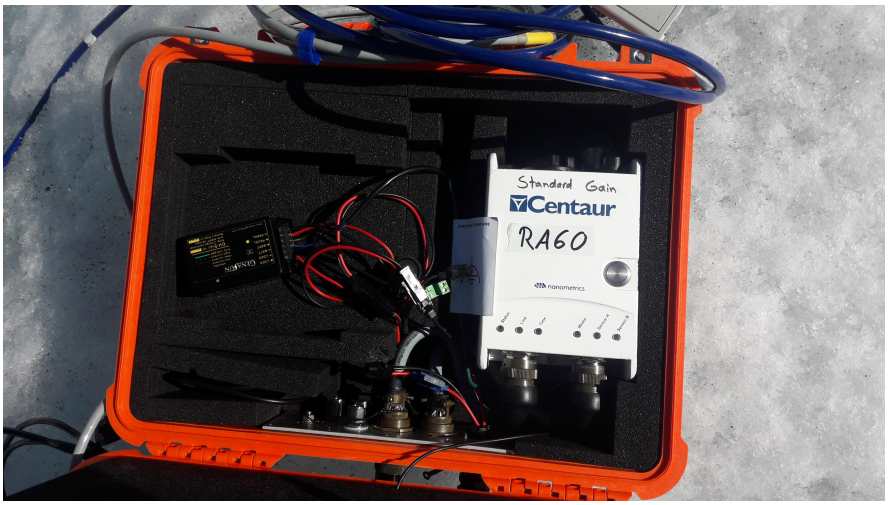

Figure 4: An example of content of the pelicase of a seismic station. The most important items are the digitiser (in this case a Nanometrics Centaur with standard gain), the battery and the GPS antenna.

On multiple occasions, the exact location of the seismic station was measured by means of a differential GPS, in order to account for their displacement caused by surface motion of the glacier.

During fieldwork in the summer of 2018, the seismometers had to be redrilled, since the melt caused them to emerge at the surface. This was done on the 9th of August for RA51 and RA52. RA53 was redrilled on the 3rd of August.

Figure 5: An example of the installed borehole seismometers. They were installed four meters into the ice. The blue cable is attached to the pelicase with the digitiser.

2.3 Data Processing and Analyses

This research studies the data starting from 30-09-2017 at 00:00:00 until 22-08-2018 at 23:59:59.

In order to identify stick-slip events, a detection algorithm was used, which identifies stick-slip events from their spectral content. From all detected clusters, two are chosen to be studied in more detail, in order to narrow the scope of the research.

After their identification, the detected events were stacked and aligned in order to see how similar they were. After this, a weighted mean was taken, so that the noise cancelled and a cleaner signal remained. This could then be used as a template for an adapted cross-correlation code in order to find similar events (the weighted stacks used in this study can be seen in Appendix B). Comparable cross-correlation methods have been used in previous cryoseismological research (Dalban Canassy et al., 2016; Helmstetter et al., 2015; Roeoesli et al., 2016). For the cross-correlation method used in this study (and also the further processing of the data to produce plots), different scripts in Python were used which rested heavily on the extensions *ObsPy* (Beyreuther et al., 2010) and *EQcorrscan* (Chamberlain et al., 2017). The threshold which had to be reached to call it an event of the same cluster was first set at a normalised cross-correlation coefficient of 0.50,

which is approximately the same as was also used in other studies (Dalban Canassy et al. (2016); Helmstetter et al. (2015): 0.5; Roeoesli et al. (2016): 0.4). Helmstetter et al. (2015) found that the number of false detections increased drastically when the correlation coefficient was set at 0.4.

Detected events were later scanned through by hand in order to discard false detections. These were recognised based on differences in the relative arrival times of P- and S-waves between the three stations (which would indicate a different source location), significantly different waveforms or incorrect polarities.

There were a few problems encountered during the cross-correlations. Close to RA53, a *moulin* opened (a hole in which the meltwater drained). This produced a lot of noise in the data, which can be seen in the produced stacks in Appendix C.

Furthermore, the seismometers were redrilled (RA51 and RA52 on the 9th of August 2018, RA53 on the 3rd of August 2018). As a consequence, the horizontal components of the seismometers were turned. Therefore, a second detection run was performed from the 20th of July onwards for which only the z-components was correlated. It was found that for this run correlation coefficients of detections were lower, so the threshold was set to 0.45 for one of the clusters (later called XX) and to 0.48 for another (later called BQ). The reason for this difference was that the number of false detections increased drastically at a higher level for BQ than for XX.

The locations of icequake asperities were computed by means of an adapted code which used the probabilistic non-linear earthquake location software NonLinLoc (Lomax et al., 2000). For this, P- and S-wave arrival times have to be picked from the data of different stations. This software package returns an uncertainty ellipse based on errors in these picking times and uncertainties in wave velocity.

In this study, a relative measurement of the maximum amplitude of a single event was calculated by checking for the largest value of the recorded waveform in each directional component of a station in the 0.3 seconds after the arrival time of the P-wave. After this, the maximum amplitude in each component was set to one and the other values were normalised with respect to this amplitude. Finally, the mean of all active components was taken as a measurement of the relative amplitude. Since two clusters have different source locations, their amplitudes can not be compared or added and are therefore treated separately.

Furthermore, an estimate of the released seismic energy per time unit was calculated from the amplitudes. Released energy scales both with the total number of events as with the square of the amplitudes (Shearer, 2009). Therefore, a rolling sum of the squared amplitudes of all events was taken over a specific time window. Again, it must be noted that the energies of two clusters do not have the same units and their values can therefore not be added.

Finally, it was chosen to correlate variables that influence melt or that are a proxy for this, in order to check the proposed hypothesis. For this, weather data (precipitation, air temperature and solar irradiation) was taken from the station at Grimsel Hospiz. Although this is not on the glacier itself, it is the closest weather station present. In the valley beneath Rhonegletscher, at the village of Gletsch, the discharge was measured with a gauge. Although the meltwater from Muttgletscher passes the gauge in Gletsch as well, the majority of water comes from Rhonegletscher and the discharge can therefore be taken as a reliable approximation for the melt on the glacier.

3 Results

3.1 Microseismic Activity

The spectral detection algorithm found between 20 and 35 clusters. Two clusters were chosen to be investigated in detail, called 'BQ' and 'XX'. These were selected based on their activity during the second fieldwork period in July and August of 2018, which made it possible to adjust the field campaign to them. The correlation method resulted in the discovery of 1762 events of cluster BQ and 532 of cluster XX. These events were checked by hand to remove false detections. In the end, 1131 events of cluster BQ and 128 events of cluster XX were detected.

From the recorded signals, the ground velocity can be computed with the given sensitivities. This led to mean ground velocities in the order of 10^3 nm/s (see table 2 in Appendix D). Furthermore, the average time between the P and S wave for both BQ and XX is approximately 0.1 seconds (see Appendix C). This is compared with recordings shown in Helmstetter et al. (2015) and Walter et al. (2009), which have roughly the same time between the P- and S-waves. The ground velocity is approximately twice as large as detected by Helmstetter et al. (2015) and an order of magnitude larger than Walter et al. (2009), which suggests the found events are larger, but still microseismic.

The locations of the two clusters were computed to be just north of the seismic stations used in this study (see figure 2). The distance between them is 65.43 meters on the map. The localisation algorithm determined that cluster BQ and XX were located at a height of 2314 +/- 15 meters and 2295 +/- 15 meters above sea level, respectively. From GPS measurements it is known that the ice surface above XX was roughly 2484 meters above sea level and for BQ it was estimated to be around 2500 meters above sea level. This results in 186 for BQ and 189 meters for XX, excluding error margins. The melt which occurred during the drilling period has to be taken into account, which is roughly 2-3 meters. Drilling efforts found that the bedrock was located at a depth of roughly 190 meters. This shows that the depth is within the errors margins. Together with the lack of Rayleigh waves in the detections, this indicates that these are indeed deep events.

To show the mixed polarities, the seismic recordings of one event from each cluster was studied by more than the three stations used in this study (see figures 13 and 14 in Appendix A). Both clusters show clearly mixed polarities. When comparing this with the map in figure 15 in Appendix A, it becomes clear that stations downstream of a cluster detect positive amplitudes of arriving P-waves, which means that they are compressional, whereas stations located upstream detect negative, dilational waves. This proves that these were indeed stick-slip events, with slip in the direction of glacier flow.

In order to check the correctness of the detections, they were stacked and aligned (see figures 18, 19 and 20 in Appendix C). Since there are some outliers in every stack and some detections might have been missed, it is estimated that the human picking error is about 5 detections per 50 detections or 10%.

By analysing the detected events, it becomes clear that cluster BQ was active starting from 17-06-2018 until 22-08-2018 (the end of the measurements)(see figure 25 in Appendix E). This is here defined as the *Active Period*. In figure 6, the activity of both clusters during this period is shown. The period when there is activity of cluster XX is limited from 18-07-2018 to 31-07-2018. An interesting observation is the large peak in the number of events of cluster BQ in the night and morning of 29-07-2018.

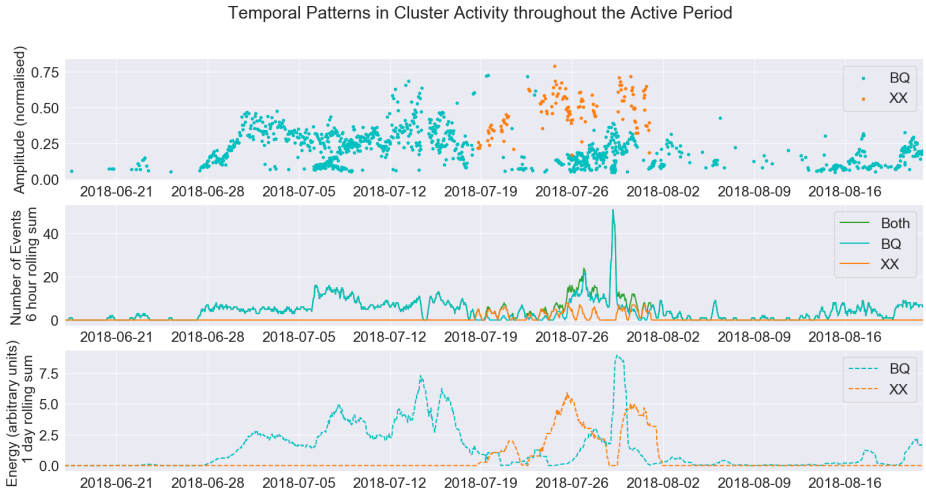

Figure 6: Activity of both clusters throughout the active period (17-06-2018 to 22-08-2018). The top graph shows the amplitude, the middle one cluster activity (6 hour sum) and the one at the bottom shows the seismic energy released in 1 day in arbitrary units. Note that amplitude and energy of both cluster do not have the same units. Time in UTC.

3.2 The Effect of External Conditions on Stick-Slip Activity

From figure 7, the daily behaviour of the clusters can be studied. What is interesting to see is that the clusters show an opposite behaviour: the majority of the events of cluster XX take place in the afternoon and evening (approximately between 12 pm and 1 am), whereas hardly any events occur during the morning and night (approximately between 2 am and 11 am). The activity of cluster XX seems to follow the curves of the average discharge systematically and lags compared to the curves for temperature and especially solar radiation. This pattern is statistically significant. Cluster BQ shows an opposite pattern. The majority of the events seem to take place in the morning and night, with a drop in activity during the afternoon. It must be noted that the uncertainty of most bars indicating higher than average activity still overlap with the mean of activity. This is less often the case for bars indicating lower than average activity.

The time series of the activity of cluster XX and the environmental parameters can be studied in figure 8. The activity of cluster XX systematically follows all variables. There is a positive correlation with the environmental parameters and a clear daily cycle present. Also the number of events per day corresponds with the environmental variables. The activity is at the same time as changes in discharge (half an hour lead) and lags three hours compared to air temperature and five hours compared to solar radiation, as suggested by cross-correlation.

The periodicity of the events can be studied by looking at the periodograms of the data (see figure 9). The events of XX show a peak at a period of 24 hours. This peak can also be found in the solar radiation, temperature and discharge curves. Unlike in figure 7, where the diurnal frequencies are amplified due to the stacking, the activity of cluster BQ does not show any clear periodicity.

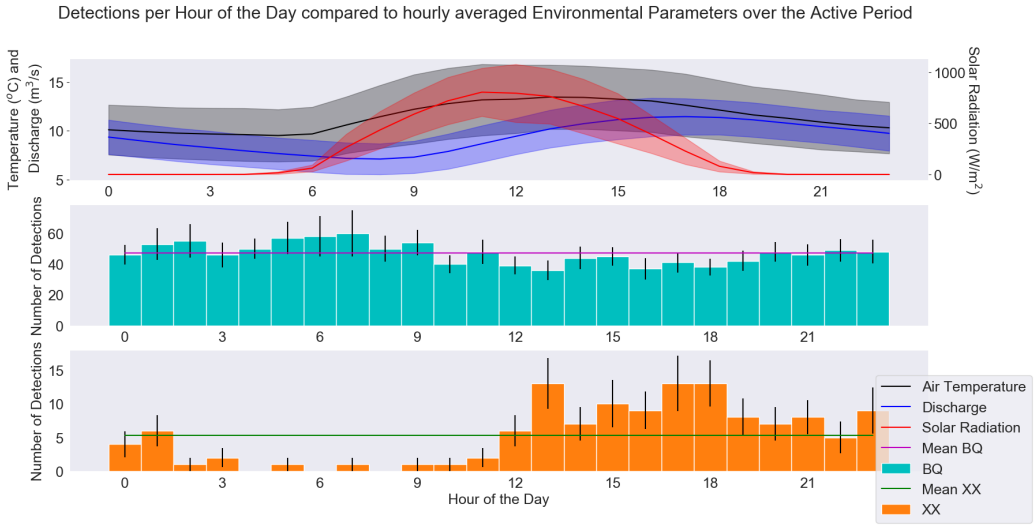

Figure 7: Average conditions of air temperature, discharge and solar radiation per hour of the day compared to the total number of detections per hour of the day throughout the active period (17-06-2018, 22-08-2018). The shaded bands in the graph at the top indicate the standard deviation, the bars in the lower graph show the sum of the deviations from the mean of the events per hour over the observation period.

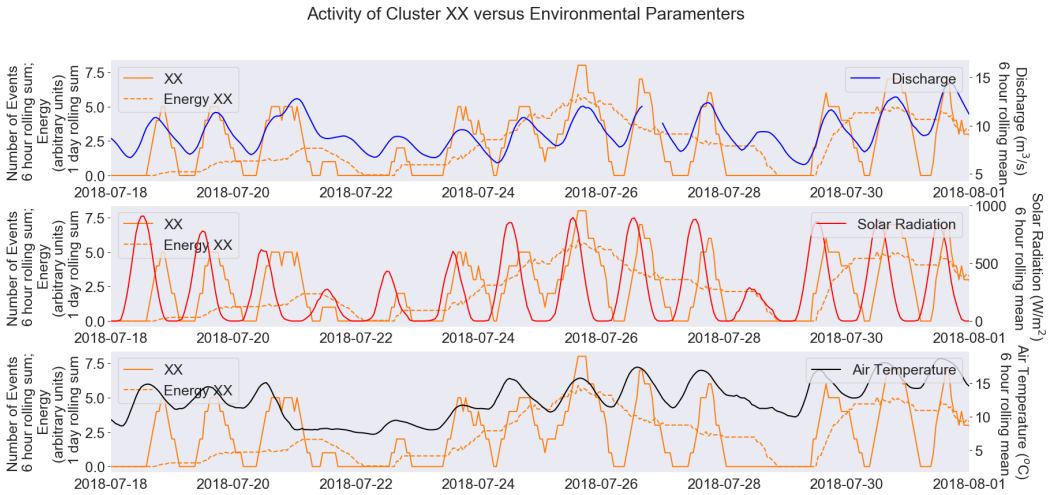

Figure 8: Activity and seismic energy of cluster XX compared to the environmental parameters (discharge, solar radiation and air temperature from top to bottom). The activity is a 6 hour rolling sum, energy is a 1 day rolling sum, environmental parameters are a 6 hour rolling mean. Time in UTC.

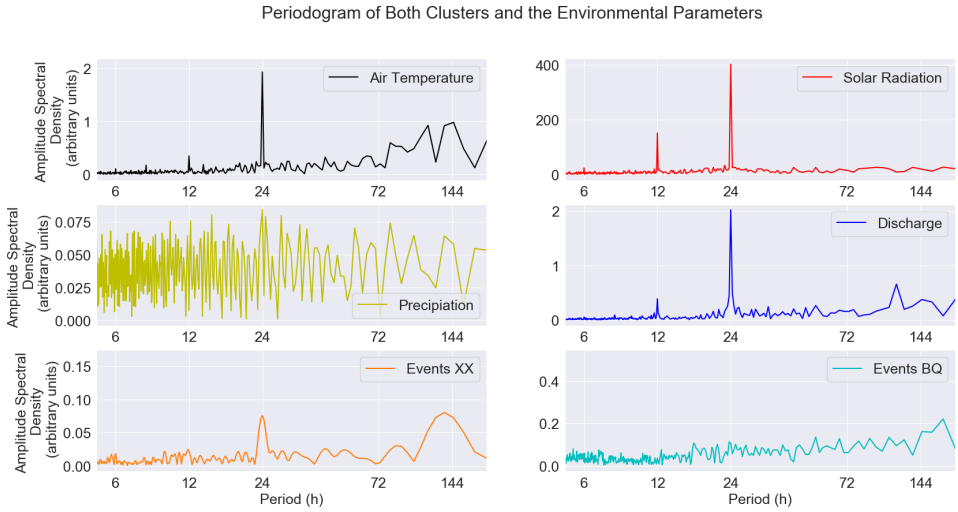

Figure 9: Periodograms for the environmental parameters and the events throughout the active period (17-06-2018, 22-08-2018). Precipitation is included, because there were many thunderstorms in the evening during the fieldwork period.

3.3 The Relation between Amplitude and Interevent Time

In a next step, the relationship between the time between two consecutive events (the *interevent time*) and the amplitude of the last event of these is studied. In the analysis, only the 90% of the detections with lowest interevent time have been taken into account, since the few detections with a much longer interevent distort the image drastically and on longer timescales processes such as viscosity start to play a dominating role (see figure 21 in Appendix D). For cluster BQ, a relation between relative amplitude and interevent time can be seen, although it remains unclear if this is linear (see figure 10 and figure 23 in Appendix D). Even though the events per hour show a relation with hour in figure 7, the hour of the day does not seem to have an effect on amplitude. For cluster BQ, there seems to be a lower limit for amplitudes between 0.05 and 0.1, below which no events were detected (see figure 22 in Appendix D). Cluster XX does not seem to show a clear positive relation between amplitude and interevent time (see figure 10). However, events that occur in the night seem to have on average a larger interevent time than events that occur at day. This does not seem to influence the amplitude. Cluster XX does not seem to have a clear lower limit for amplitudes.

The variation of amplitude and interevent time throughout the active period was also studied (see figure 11). For cluster BQ, it seems that through time, the amplitude and interevent time get smaller. However, it is pointed out that due to the fact that the detection threshold for the cross-correlation search was lowered for the end of July and August, there might be a bias, since detections with a lower amplitude coefficient seem to have a lower correlation coefficient, since the noise gets dominant (see figure 22 in Appendix D). Cluster XX shows an opposite behaviour in figure 11. The amplitude of the events increase over time.

Also, a Kernel Density Estimate on the distribution of the amplitudes and interevent times of both clusters has been done (see figure 12). Added to this figure is an Kernel Density Estimate

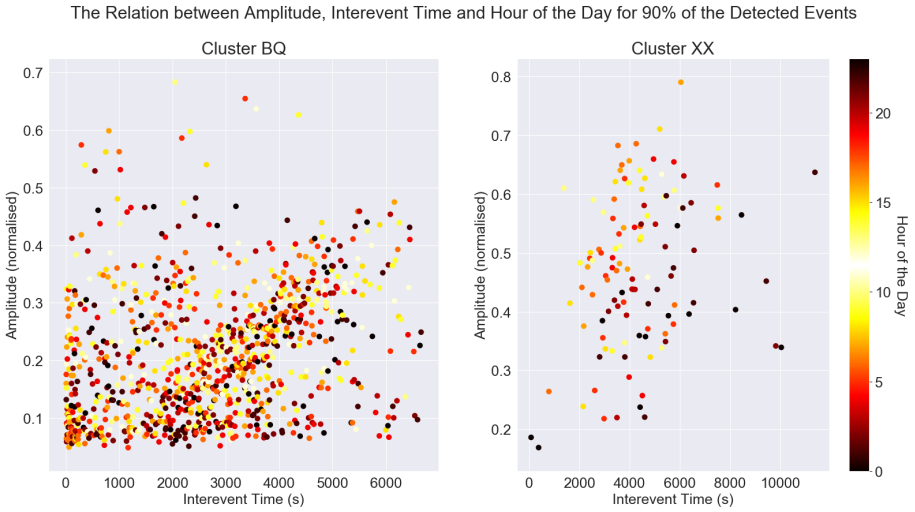

Figure 10: Amplitude (normalised to the maximum of each component of each station) compared to interevent time. For this, only the 90% detections with smallest interevent time is taken. Colours indicate the hour of the day.

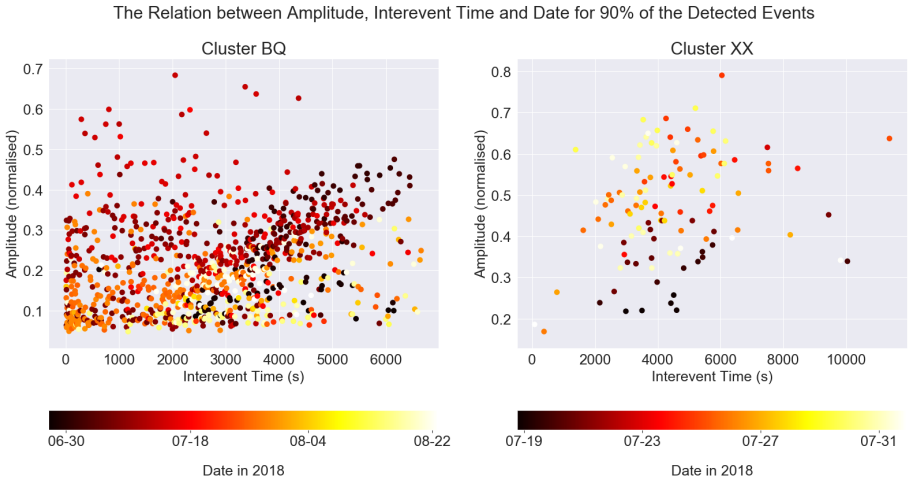

Figure 11: Amplitude (normalised to the maximum of each component of each station) compared to interevent time. For this, only the 90% detections with smallest interevent time are taken. Colours indicate the date.

for the times between an event of XX and the following event from BQ, and vice versa. What is clear from this figure is that whereas the interevent times of XX show a clear unimodal behaviour, the BQ is bimodal. The mode of XX is larger than both of BQ. Interestingly, the mode of the

intercluster interevent times are both at the same location as the minimum between the two modes of BQ. The amplitude of cluster BQ also displayes a somewhat bimodal behaviour. The amplitude of cluster XX is unimodal. The relative shift in amplitudes can not be interpreted, due to the different normalisations.

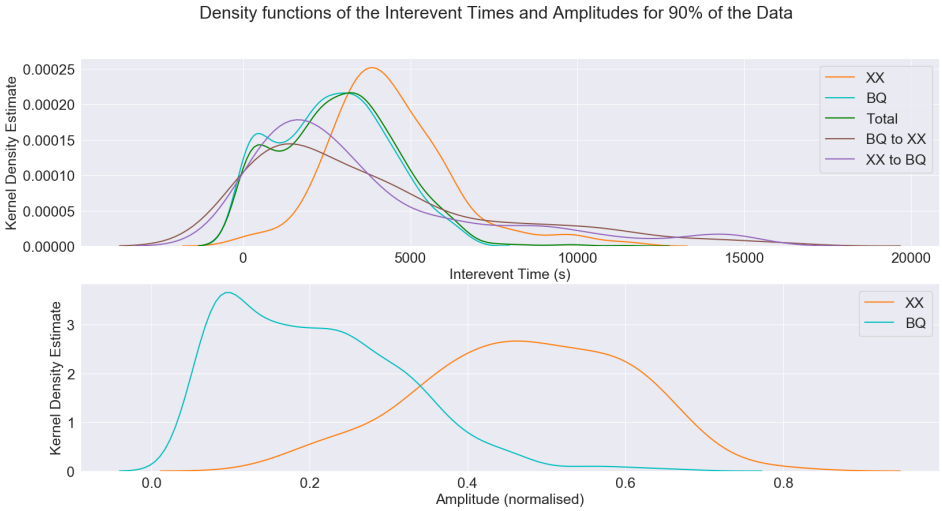

Figure 12: Kernel Density Estimates for amplitude and interevent time for both cluster BQ and XX. Also interevent time between one event of one cluster and the consecutive event of the other cluster is shown.

4 Discussion

In the previous section, the activity of clusters BQ and XX has been analysed. A strong correlation between the activity of cluster XX and the environmental parameters that describe melt was shown. Plotting the interevent times versus the amplitude showed a positive relationship for cluster BQ. In the following sections, these two main results will be interpreted and compared with existing literature. Finally, the possibility of interaction between the two clusters will be studied.

4.1 Timing of the Events

The presented data suggest a different behaviour for cluster XX than for cluster BQ. The activity of cluster XX seems to be strongly influenced by the daily 24 hour cycle of temperature and radiation, as suggested by the time series in figures 7 and 8 and the periodograms in figure 9. The lag of cluster activity to temperature and solar radiation hint towards a causal relationship. The activity leads the discharge by half an hour, which is due to the gauge's location at Gletsch, so that it takes longer for changes in melt to be recorded. Together, these correlations point to surface melt as a mechanism, although correlation does not necessarily imply a causality. Interestingly, cluster BQ does not seem to be influenced strongly by the studied environmental parameters. Although figure 7 seems to suggest some kind of a daily 24 hour cycle with higher activity in the morning and night, albeit with low statistical certainty, this behaviour can not be observed in the periodograms in figure 9. The daily variation of BQ might be strongly influenced the peak in activity on the 29th of July, which takes place only in the night and morning. When studying the time series of cluster BQ and the environmental parameters, no clear correlation to any of the parameters can be seen (see figure 26 in Appendix E).

Previous research has also studied diurnal variations in the occurence of icequakes. Both strong (Thelen et al., 2013; Walter et al., 2008) and no diurnal variations in behaviour (Helmstetter et al., 2015) have been observed. At a glacier on Mount Rainier (USA), a cluster was detected that had strong diurnal variations like cluster XX, but these lagged approximately 6 hours to daily temperature variations, whereas cluster XX lags only 2 hours (Thelen et al., 2013). At Gornergletscher, two types of strong diurnal variations were found (Walter et al., 2008). The first was that total seismic activity was high in the afternoon and low in the night and morning. This is a similar behaviour as cluster XX shows. It was hypothesised that the increase in seismic activity during the day at Gornergletscher was due to the fact that the glacier reaches its maximum velocity during the day, since basal meltwater led to increased basal sliding (Walter et al., 2008). Interestingly, this variation was indeed contemporary with variations in basal water pressure. The observed correlation for cluster XX makes this mechanism likely, but direct measurements of water pressure are needed to further prove this.

For earthquakes similar mechanisms are known. In order to change from a stable sliding regime to unstable sliding (stick-slip), one of two conditions must be met: either the normal stress must become greater than the frictional strength or there must be a sudden jump in sliding velocity (Scholz, 1998). The influx of meltwater to the asperity affects both. Experiments for earthquakes have shown that lubrication of fault surfaces by fluids lead to a reduction of 30% of the frictional stress compared to situation with hydrostatic pore pressure and 50% compared to dry rock (Brodsky and Kanamori, 2001). Less frictional stress would mean that slip would occur at a lower stress, which would explain the increase in the number of events of cluster XX during the day. An increase in velocity can occur due to increased basal sliding.

However, this hypothesis was not supported for the detected basal icequakes at Gornergletscher, which showed the second type of strong diurnal variations (Walter et al., 2008). Their activity did show an active phase in the morning and night. This corresponds more to the pattern cluster BQ shows in figure 7, although these variations, if statistically significant, are not as strong. The activity of these basal icequakes was coupled to diurnal changes in glacier movement (Walter et al., 2008). It must be noted, however, that the studied basal icequakes at Gornergletscher were related to tensile faulting instead of stick-slip behaviour and might therefore be controlled by different factors.

Snow loading is another factor to which stick-slip events have been linked (Allstadt and Malone, 2014; Thelen et al., 2013). At the Mount Rainier volcano, it was found that peaks in icequake activity lagged 1 to 2 days behind precipitation. The proposed mechanism was that the extra weight from snow loading and subglacial hydrological changes from meltwater could lubricate parts of the glacier-bed interface, leading to increased activity. The clusters studied in this thesis are only active during summer, which makes an explanation involving snow loading unlikely. From the time series, no influence of precipitation could be found (see figure 27 in Appendix E).

On intermediate time scales (days and weeks), activity of cluster BQ is characterised by more active and more quiet phases. This was also observed by Helmstetter et al. (2015). This study contributed it to changes in debris concentration in the basal ice. This hypothesis, which does not invoke environmental parameters, could explain the unpredictability of cluster BQ.

Although events of cluster BQ were still detected at the end of the studied period, cluster XX seems to suddenly halt all its activity. No rapid changes in the environmental parameters that controlled its behaviour can be observed. Cluster XX has been active for approximately two weeks. At Mount Rainier in 2010, stick-slip cluster were also only active for a short period (three weeks; Thelen et al. (2013)). The fact that both clusters in that study stopped, one while pseudoenergies were increasing and one when the frequency of large events had decreased, shows that clusters can stop under different circumstances and for reasons not yet understood. Since it was tried to drill into cluster XX in August 2018, a possible explanation is that this disturbed the conditions necessary for stick slip events. However, the likelihood of this must be studied statistically before this can be concluded.

When looking beyond the active period to the activity of the entire year, it seems that both clusters become only active when temperatures, solar radiation and melt are rising in spring. Although this might very well be true, especially when activity depends on meltwater, this can not be supported by the presented data, since clusters were picked based on their activity during the fieldwork period in the summer of 2018. Other clusters were already active before this time and other studies have found cluster activity during winter (Allstadt and Malone, 2014). In order to study this yearly variability, all or at least more clusters must be taken into account and studied longitudinally for multiple years.

4.2 Amplitude and Interevent Time

Also regarding amplitude and interevent time, both clusters behave differently. For cluster BQ, it is clear that a positive relationship exists between these variables (see figure 10 and figure 23 in Appendix D). Positive relationships between interevent times and amplitude (Helmstetter et al., 2015), pseudoenergy (scales with amplitude squared) (Allstadt and Malone, 2014) and magnitude (Zoet et al., 2012) have been observed at other glaciers as well. This positive relation shows what is expected when a somewhat constant stress exerted by the movement of the glacier

accumulates at the asperity, so that when there is more time between to events, more stress has accumulated. Therefore more energy can be released, causing the event to have a larger amplitude. This corresponds to the slip-predictable model (Shearer, 2009). Deviations from this relation indicate that the built up stress from the glacier's sliding velocity changes during the time or that asperity only releases part of the stress, the rest being released by basal sliding (Helmstetter et al., 2015). Whereas the correlation at Glacier d'Argentière was only visible up to interevent times of 25 minutes (Helmstetter et al., 2015), the correlation for cluster BQ is clearly visible up to an interevent time of approximately 85 minutes (5000 seconds; see figure 10).

Cluster XX does not show a strong relation between amplitude and interevent time. This might partly be due to the lack of observed events. However, it does show an interesting dependence on the hour of the day (see figure 10). Regardless of amplitude, the interevent time seems to decrease from night to day. This is logical when taking into account that the cluster activity largely takes places during the day, so that the smaller number of events occurring during the night have more time between them.

Both clusters seem to show a change over time with regard to amplitudes and interevent times (see figure 11). The amplitudes and interevent times for cluster BQ seem to decrease over time. It has to be noted that there is a bias, since smaller amplitudes correlate with lower correlation coefficients, and the correlation threshold was set lower for the end of July and the whole of August (see figure 22 in Appendix D). However, the trend already seems to start before this time, which suggests that it is real. A decreasing amplitude over time can indicate multiple things. One option would be that less energy is released via this cluster. When looking at the energy released over time, this indeed seems to happen (see figure 6). A large exception is the peak at the end of July. Another possible explanation might be that the asperity can support less stress and slips easier. This would correspond with more events, which all have lower amplitudes, since the accumulated stress is less. Signs for this are the fact that the highest peaks in activity are at the end of July. This decrease in frictional strength of the asperity might be caused by more lubrication due to meltwater, analogous to earthquakes (Brodsky and Kanamori, 2001). Also at Glacier d'Argentière, differences in peak amplitude over time were discovered. Here, it was hypothesised that this was the result of changing debris concentrations in basal ice (Helmstetter et al., 2015), which might also be an explanation.

At Mount Rainier, changes in the relationship between interevent times and pseudoenergy were also studied and it was found that for short periods, this relation was linear (Allstadt and Malone, 2014). However, over time this slope changed, which correlated with additional snowfall. On average, there was a trend towards an increase in frequency of small events and less larger events. The interevent time tended to increase over time, so the slope of the graph became flatter over time. When looking at only the youngest data of BQ, it does indeed seem like it is flattening off, although this cannot be stated with great certainty. The slope between amplitude and interevent time over time can be taken as a measure for slip rate, if it is assumed that the fault size does not change over time (Allstadt and Malone, 2014). This would suggest that the stress posed by Rhonegletscher is decreasing over time for cluster BQ.

Cluster XX seems to show quite the opposite pattern compared to cluster BQ. The amplitude seems to increase over time (see figure 11). In figure 6, it is shown that the energy release increases even though the total number of events per time unit does not increase drastically, suggesting that more energy is released via this cluster over less events.

When comparing the distribution of interevent times for each cluster, it shows that on average the times of cluster XX are larger than those of BQ (see figure 12). Furthermore, whereas cluster XX shows a unimodal distribution, cluster BQ is bimodal. The distribution of amplitudes of cluster BQ also hints towards bimodality. Signs for this bimodality can also be seen in figure 10, which shows a relatively high concentration at short interevent times and low amplitudes. It might be the case that the peak at lower amplitudes corresponds to the peak of shorter interevent times, since less stress was built up.

Interestingly, there is some similarity in behaviour with what was found at Mount Rainier in 2010 (Thelen et al., 2013). There, it was also found that the cluster that was active for a longer time and showed no diurnal variations had shorter interevent times than the cluster showing diurnal activity. It was further found that range between the highest and lowest pseudoenergy level of the diurnally active cluster was much narrower. This might also be the case for the clusters in this study, since the amplitude values of XX are much closer to their maximum (as suggested by figures 6 and 12). Future research can compute the seismic magnitude of the cluster in this study in order to check this.

4.3 Interaction between Clusters

An interesting object of studying is possible interaction between the two clusters. Due to their proximity to each other, a hypothesis for this might be that the energy that accumulates due to the build up of stress is divided over the two cluster when released. Evidence in support of this hypothesis can be seen in figure 6. Before cluster XX becomes active, the amount of energy released by cluster BQ per time unit drops. Furthermore, cluster BQ reaches maximum energy release per time unit exactly when the energy release of cluster XX reaches a minimum. The fact that the energy released by cluster BQ is not constant in the time period before XX is active, may be explained by the energy release by other active clusters which were not accounted for in this study. The drop to no energy release in most of August might be explained the same way, or other factors, such as sliding due to increased meltwater production, might release the energy. Since the estimates for energy of both clusters use different arbitrary units, they can not be added to see if the released energy remains roughly constant when both are active.

Another way in which the clusters could possibly interact, is that the activity of one cluster triggers the activity of the other. Direct triggering due to passing seismic waves is known for earthquakes (Hill et al., 1993). However, due to the proximity of the asperities of cluster BQ and XX, this will be hard to measure, since the wave signals will arrive virtually simultaneous at the stations, making them hard to detect separately. In this study, no interevent times smaller than 11 seconds have been observed, which might indicate that direct triggering did not take place or that it was not possible to observe this with the method used. Triggering can also happen on longer timescales: an event of one cluster might destabilise another location, which might respond to this. At Parkfield, California, it has been observed that microearthquakes which were 100 to 200 m apart showed a peak in interevent time distribution at interval smaller than 10 minutes (Nadeau et al., 1995). This indicated that these earthquakes were communicating with velocities of 10 to 100 cm/s. Nadeau et al. (1995) suggested rapid aseismic slip or stress field perturbations as a possible mechanism for this. Helmstetter et al. (2015) studied triggering between stick-slip icequakes on times scales of several minutes, but found no interaction due to triggering. The cumulative distribution of interevent times between the two clusters were compared to a Poisson distribution, in order to find how random these were (see figure 24 in Appendix D). It was found that for BQ to XX, more shorter interevent times were present than

would be expected by a Poisson distribution. For XX to BQ, the reverse was true. Although it is hard to tell the statistical significance of this, this would suggest that triggering on a minute scale does take place from BQ to XX.

However, the fact that the number of events of one cluster seems to go down when the other cluster is active and that the correlation between the activity of cluster BQ and XX over time are slightly negative suggests that triggering of other clusters is not a dominant mechanism behind observed cluster activity.

5 Conclusion

This thesis analyses the behaviour of two stick-slip clusters on Rhonegletscher through time. The two clusters studied show different behaviour. The strong diurnal variations in activity of cluster XX, which follow the changes in discharge, suggest an underlying mechanism influenced by changes in subglacial hydrology, which change basal water pressures and stresses around asperities. This corresponds with the proposed hypothesis. However, cluster BQ does not show this dependency on external controls. Future studies are needed to find out what internal changes determine its behaviour.
The activity of cluster BQ shows clearly that the amplitude of events become larger when interevent times increase, in accordance with the hypothesis. This indicates that there is a relatively constant amount of stress accumulation. It remains an open question how much of the basal sliding of the glacier is accounted for by stick-slip.
Direct triggering between events does not seem to take place, although there might be activation with some time delay between BQ and XX. From the presented time series, it might be possible that the energy that accumulates from stress is divided over both clusters, since the activity of one cluster seems to increase when the other cluster becomes less active. If this is the case, it might be interesting to involve more clusters to see if this can also be shown on a larger scale.

This thesis is only a first investigation of these relations. Future research can use the presented results as a guide for a larger and more thorough study, spanning multiple years and analysing more stick-slip clusters, while considering more external variables such as basal water pressure, glacier flow velocity and snowfall. The results of this study suggest a strong dependence of cluster activity on melt and on stress imposed by the glacier. These are both sensitive to changes in climate and it is therefore probable that the activity of stick-slip clusters will change in the future.

References

Allstadt, K. and Malone, S. D. (2014). Swarms of repeating stick-slip icequakes triggered by snow loading at Mount Rainier volcano. *Journal of Geophysical Research: Earth Surface*, 119(5):1180–1203.

Beyreuther, M., Barsch, R., Krischer, L., Megies, T., Behr, Y., and Wassermann, J. (2010). Obspy: A Python toolbox for seismology. *Seismological Research Letters*, 81(3):530–533.

Bindschadler, R. A., King, M. A., Alley, R. B., Anandakrishnan, S., and Padman, L. (2003). Tidally controlled stick-slip discharge of a West Antarctic ice. *Science*, 301(5636):1087–1089.

Brodsky, E. E. and Kanamori, H. (2001). Elastohydrodynamic lubrication of faults. *Journal of Geophysical Research: Solid Earth*, 106(B8):16357–16374.

Chamberlain, C. J., Hopp, C. J., Boese, C. M., Warren-Smith, E., Chambers, D., Chu, S. X., Michailos, K., and Townend, J. (2017). EQcorrscan: Repeating and near-repeating earthquake detection and analysis in python. *Seismological Research Letters*, 89(1):173–181.

Cuffey, K. M. and Paterson, W. S. B. (2010). *The physics of glaciers*. Academic Press.

Dalban Canassy, P., Roeoesli, C., and Walter, F. (2016). Seasonal variations of glacier seismicity at the tongue of Rhonegletscher (Switzerland) with a focus on basal icequakes. *Journal of Glaciology*, 62(231):18–30.

Doyle, H. A. (1995). *Seismology*. Wiley.

Farinotti, D., Huss, M., Bauder, A., Funk, M., and Truffer, M. (2009). A method to estimate the ice volume and ice-thickness distribution of alpine glaciers. *Journal of Glaciology*, 55(191):422–430.

Fischer, M., Huss, M., and Hoelzle, M. (2015). Surface elevation and mass changes of all Swiss glaciers 1980–2010. *The Cryosphere*, 9(2):525–540.

Gabbi, J., Carenzo, M., Pellicciotti, F., Bauder, A., and Funk, M. (2014). A comparison of empirical and physically based glacier surface melt models for long-term simulations of glacier response. *Journal of Glaciology*, 60(224):1140–1154.

Glaciological Reports (1881-2017). The Swiss Glaciers. *Yearbooks of the Cryospheric Commission of the Swiss Academy of Sciences (SCNAT) published since 1964 by the Labratory of Hydraulics, Hydrology and Glaciology (VAW) of ETH Zürich*, (1-136).

Helmstetter, A., Nicolas, B., Comon, P., and Gay, M. (2015). Basal icequakes recorded beneath an Alpine glacier (Glacier d'Argentière, Mont Blanc, France): Evidence for stick-slip motion? *Journal of Geophysical Research: Earth Surface*, 120(3):379–401.

Hill, D., Reasenberg, P., Michael, A., Arabaz, W., Beroza, G., Brumbaugh, D., Brune, J., Castro, R., Davis, S., Depolo, D., et al. (1993). Seismicity remotely triggered by the magnitude 7.3 landers, california, earthquake. *Science (New York, NY)*, 260(5114):1617–1623.

Huss, M. and Farinotti, D. (2012). Distributed ice thickness and volume of all glaciers around the globe. *Journal of Geophysical Research: Earth Surface*, 117(F4).

Jouvet, G., Huss, M., Blatter, H., Picasso, M., and Rappaz, J. (2009). Numerical simulation of Rhonegletscher from 1874 to 2100. *Journal of Computational Physics*, 228(17):6426–6439.

Lomax, A., Virieux, J., Volant, P., and Berge-Thierry, C. (2000). Probabilistic earthquake location in 3d and layered models. In *Advances in seismic event location*, pages 101–134. Springer.

Mercanton, P.-L., Heim, A., Held, L., and Rütimeyer, L. (1916). *Vermessungen am Rhonegletscher: Mensurations au glacier du Rhône. 1874-1915*. Zürcher & Furrer.

Moore, P. L., Winberry, J. P., Iverson, N. R., Christianson, K. A., Anandakrishnan, S., Jackson, M., Mathison, M. E., and Cohen, D. (2013). Glacier slip and seismicity induced by surface melt. *Geology*, 41(12):1247–1250.

Nadeau, R. M., Foxall, W., and McEvilly, T. (1995). Clustering and periodic recurrence of microearthquakes on the San Andreas fault at Parkfield, California. *Science*, 267(5197):503–507.

Neckel, N., Loibl, D., and Rankl, M. (2017). Recent slowdown and thinning of debris-covered glaciers in south-eastern Tibet. *Earth and Planetary Science Letters*, 464:95–102.

Podolskiy, E. A. and Walter, F. (2016). Cryoseismology. *Reviews of geophysics*, 54(4):708–758.

Pomeroy, J., Brisbourne, A., Evans, J., and Graham, D. (2013). The search for seismic signatures of movement at the glacier bed in a polythermal valley glacier. *Annals of Glaciology*, 54(64):149–156.

Rignot, E. and Kanagaratnam, P. (2006). Changes in the velocity structure of the Greenland Ice Sheet. *Science*, 311(5763):986–990.

Ritz, C., Edwards, T. L., Durand, G., Payne, A. J., Peyaud, V., and Hindmarsh, R. C. (2015). Potential sea-level rise from Antarctic ice-sheet instability constrained by observations. *Nature*, 528(7580):115.

Roeoesli, C., Helmstetter, A., Walter, F., and Kissling, E. (2016). Meltwater influences on deep stick-slip icequakes near the base of the Greenland Ice Sheet. *Journal of Geophysical Research: Earth Surface*, 121(2):223–240.

Roethlisberger, H. (1972). Seismic exploration in cold regions.

Scambos, T. A., Bohlander, J., Shuman, C. u., and Skvarca, P. (2004). Glacier acceleration and thinning after ice shelf collapse in the Larsen B embayment, Antarctica. *Geophysical Research Letters*, 31(18).

Scholz, C. H. (1998). Earthquakes and friction laws. *Nature*, 391(6662):37.

Shearer, P. M. (2009). *Introduction to seismology*. Cambridge University Press.

Smith, A. (2006). Microearthquakes and subglacial conditions. *Geophysical Research Letters*, 33(24).

Sugiyama, S., Tsutaki, S., Nishimura, D., Blatter, H., Bauder, A., and Funk, M. (2008). Hot water drilling and glaciological observations at the terminal part of Rhonegletscher, Switzerland in 2007. *Bulletin of Glaciological Research*, 26:41–47.

Sugiyama, S., Yoshizawa, T., Huss, M., Tsutaki, S., and Nishimura, D. (2011). Spatial distribution of surface ablation in the terminus of Rhonegletscher, Switzerland. *Annals of Glaciology*, 52(58):1–8.

Thelen, W. A., Allstadt, K., De Angelis, S., Malone, S. D., Moran, S. C., and Vidale, J. (2013). Shallow repeating seismic events under an alpine glacier at Mount Rainier, Washington, USA. *Journal of Glaciology*, 59(214):345–356.

Tsutaki, S., Nishimura, D., Yoshizawa, T., and Sugiyama, S. (2011). Changes in glacier dynamics under the influence of proglacial lake formation in Rhonegletscher, Switzerland. *Annals of Glaciology*, 52(58):31–36.

Wallinga, J. and Van De Wal, R. S. (1998). Sensitivity of Rhonegletscher, Switzerland, to climate change: experiments with a one-dimensional flowline model. *Journal of Glaciology*, 44(147):383–393.

Walter, F., Clinton, J. F., Deichmann, N., Dreger, D. S., Minson, S. E., and Funk, M. (2009). Moment tensor inversions of icequakes on Gornergletscher, Switzerland. *Bulletin of the Seismological Society of America*, 99(2A):852–870.

Walter, F., Deichmann, N., and Funk, M. (2008). Basal icequakes during changing subglacial water pressures beneath Gornergletscher, Switzerland. *Journal of Glaciology*, 54(186):511–521.

Weertman, J. (1957). On the sliding of glaciers. *Journal of glaciology*, 3(21):33–38.

Wiens, D. A., Anandakrishnan, S., Winberry, J. P., and King, M. A. (2008). Simultaneous teleseismic and geodetic observations of the stick-slip motion of an Antarctic ice stream. *Nature*, 453(7196):770.

Zoet, L., Carpenter, B., Scuderi, M., Alley, R., Anandakrishnan, S., Marone, C., and Jackson, M. (2013). The effects of entrained debris on the basal sliding stability of a glacier. *Journal of Geophysical Research: Earth Surface*, 118(2):656–666.

Zoet, L. K., Anandakrishnan, S., Alley, R. B., Nyblade, A. A., and Wiens, D. A. (2012). Motion of an Antarctic glacier by repeated tidally modulated earthquakes. *Nature Geoscience*, 5(9):623.

A Detections using Extra Stations

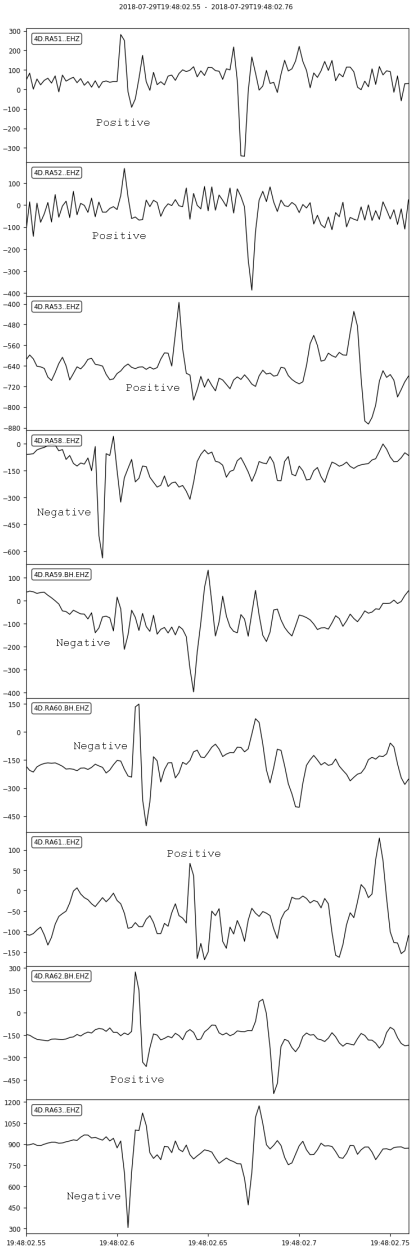

Figure 13: Unfiltered waveforms of a detection of cluster BQ at 29-07-2018 by the Z-components of 6 stations. On the y-axis, the station names are indicated and the amplitude in counts. In the figure, the polarity of the arriving P-waves are indicated. When comparing this with figure 15, it becomes clear that the downstream stations detect a compressional (positive) P-wave and the upstream ones a dilational.

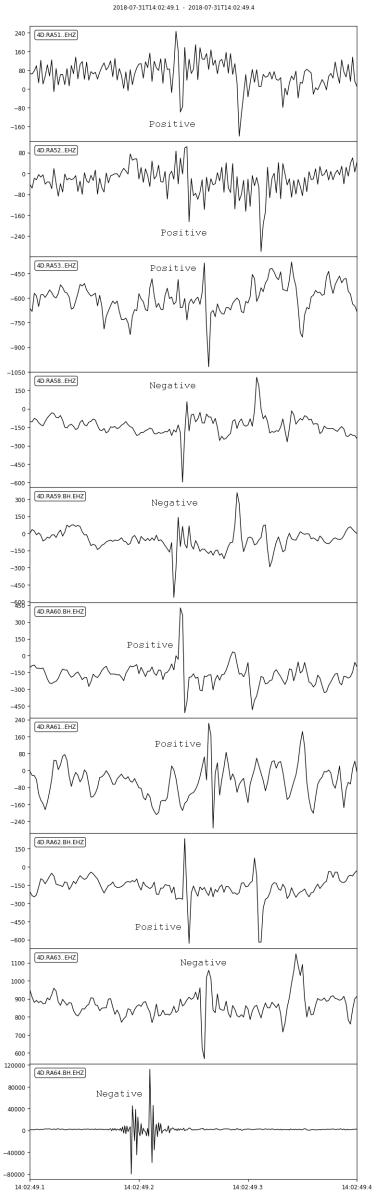

Figure 14: Unfiltered waveforms of a detection of cluster XX at 31-07-2018 by the Z-components of 6 stations. On the y-axis, the station names are indicated and the amplitude in counts. In the figure, the polarity of the arriving P-waves are indicated. When comparing this with figure 15, it becomes clear that the downstream stations detect a compressional (positive) P-wave and the upstream ones a dilational. The displayed time is longer than in figure 13, in order to include the borehole geophone, since the seismic waves reach this sensor earlier.

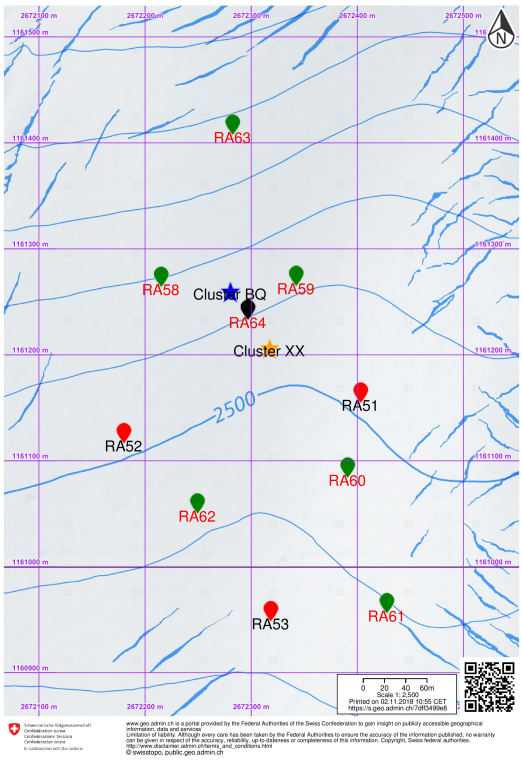

Figure 15: Map showing the locations of the stations and the clusters on 31-07-2018 (note that the seismic stations move with the glacier). Red stations are the ones used in this thesis. The green stations have been deployed during the field work in July and August of 2018. The black station has a borehole geophone at depth. Source: swisstopo.

B Stacks used for Correlation

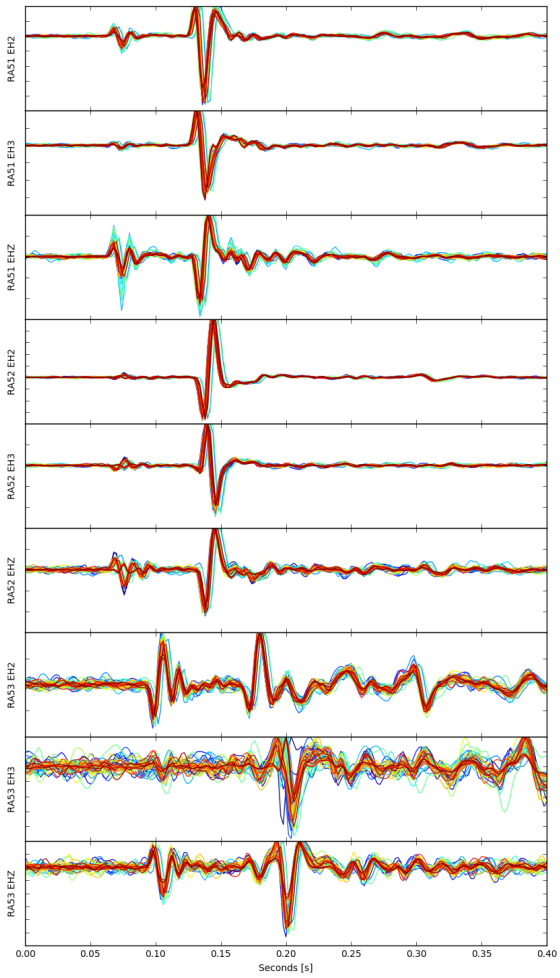

Figure 16: A filtered (bandpass between 10 and 120 Hz) and aligned stack of multiple seismic events from cluster BQ. From this stack, weighted mean was taken and used as a template. The y-axis shows the different stations with their components, with the amplitudes scaled so they all have the same size. The x-axis shows time. Note the clear positive polarity in the P-waves in the EHZ components of all stations. However, the polarity in a detections with more stations shows that it clearly has mixed polarity (see figure 13) and is therefore a basal stick-slip event.

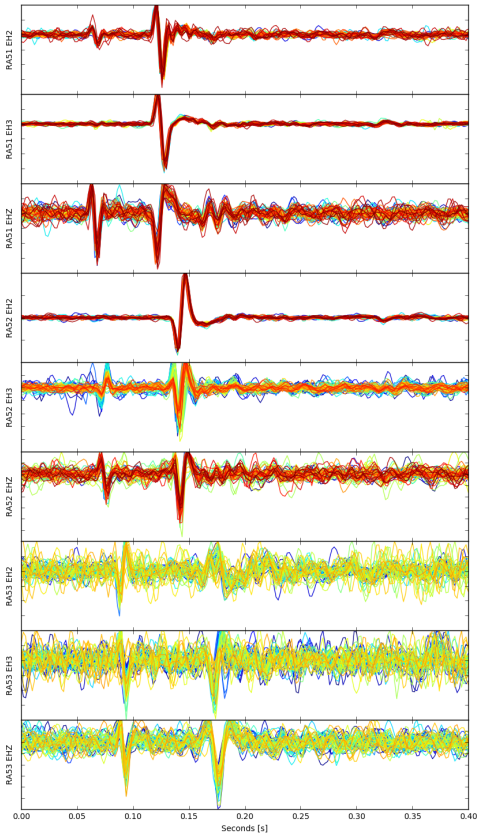

Figure 17: A filtered (bandpass between 10 and 120 Hz) and aligned stack of multiple seismic events from cluster XX. From this stack, weighted mean was taken and used as a template. The y-axis shows the different stations with their components, with the amplitudes scaled so they all have the same size. The x-axis shows time. Note the clear positive polarity in the P-waves in the EHZ components of all stations. However, the polarity in a detections with more stations shows that it clearly has mixed polarity (see figure 14) and is therefore a basal stick-slip event.

C Stacks of Detections

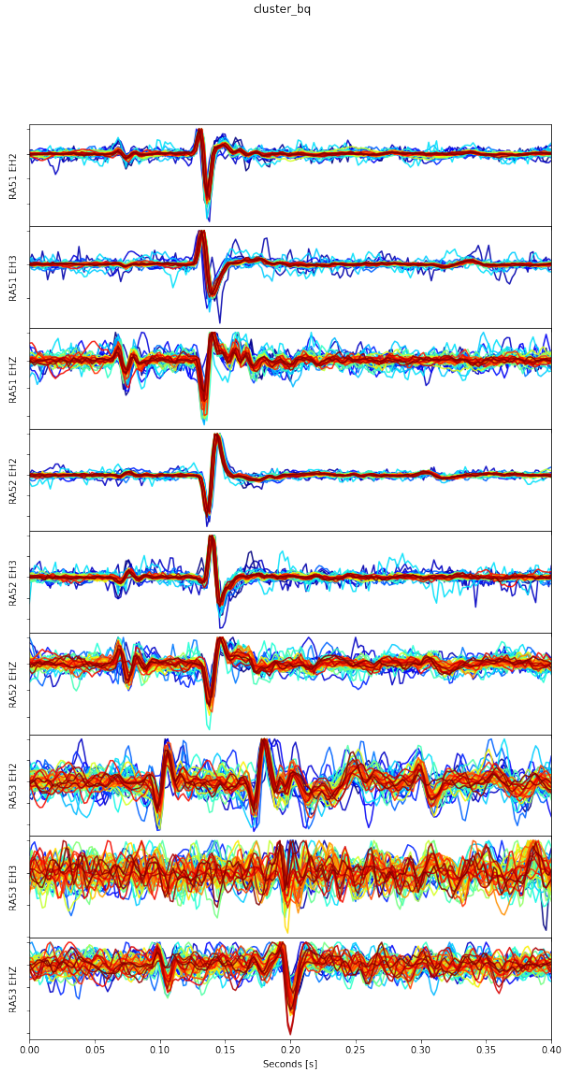

Figure 18: A filtered (bandpass between 10 and 120 Hz) and aligned stack of 50 seismic events from cluster BQ. The y-axis shows the different stations with their components, with the amplitudes scaled so they all have the same size. The x-axis shows time. In general, the events seem to align and overlap relatively well.

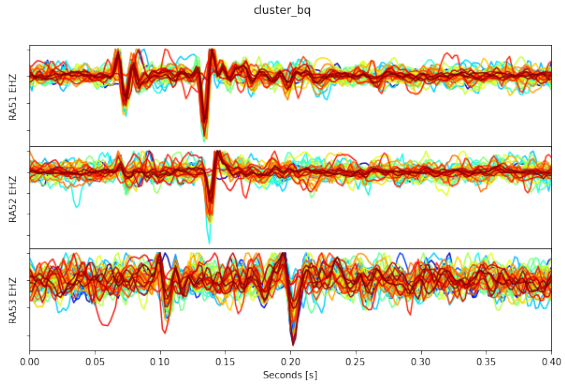

Figure 19: A filtered (bandpass between 10 and 120 Hz) and aligned stack of 50 seismic events from cluster BQ from the period where both full waveform and only the Z-components were used. Only the Z-components of the detections are shown. The y-axis shows the different stations, with the amplitudes scaled so they all have the same size. The x-axis shows time.

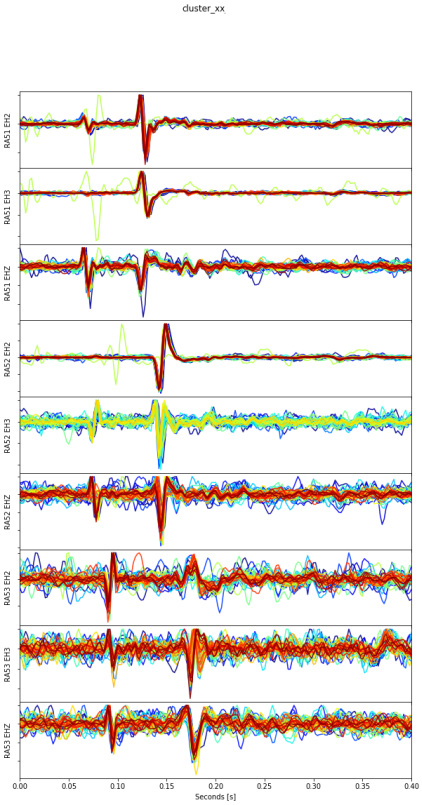

Figure 20: A filtered (bandpass between 10 and 120 Hz) and aligned stack of 50 seismic events from cluster XX. On the y-axis it shows the different stations with their components, with the amplitudes scaled so they all have the same size. On the x-axis, it shows time. The events seem to align well, with only the light green line being an outlier.

D Amplitude versus Interevent Time

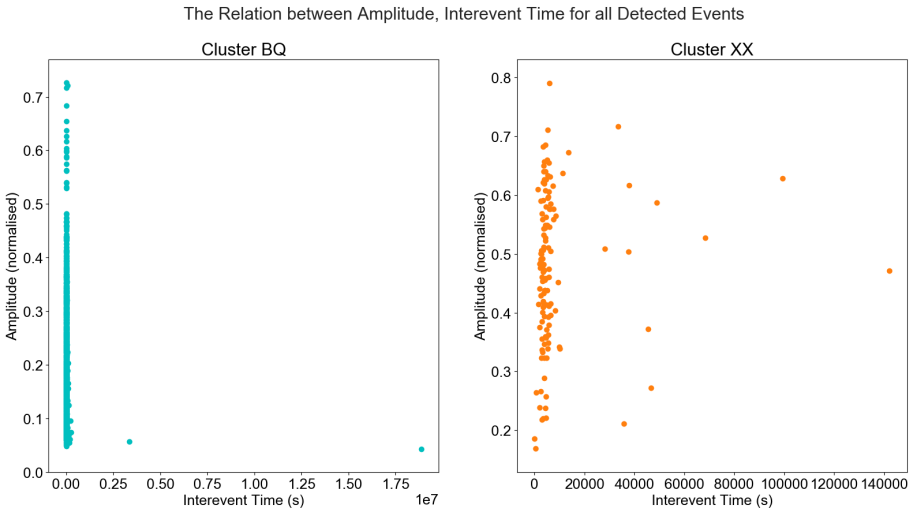

Figure 21: The relation between amplitude and interevent time for all data. Since some interevent times are extremely large, these distort the image. A reason for this might be that the stress is released by other clusters or absorbed by viscosity. Therefore, these are neglected in the data analysis part of the thesis, where only the 90% of the data with smallest interevent time is studied.

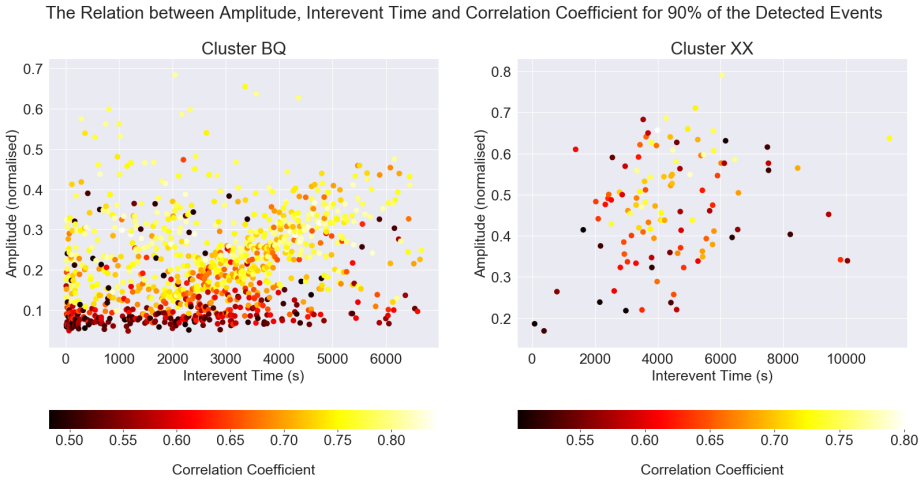

Figure 22: The relation between amplitude, interevent time and correlation coefficients for 90% of the data. For cluster BQ, it is clear that the correlation coefficient becomes lower when the amplitude decreases. Therefore, the lower limit is probably a result of our detection algorithm rather than a real physical limit.

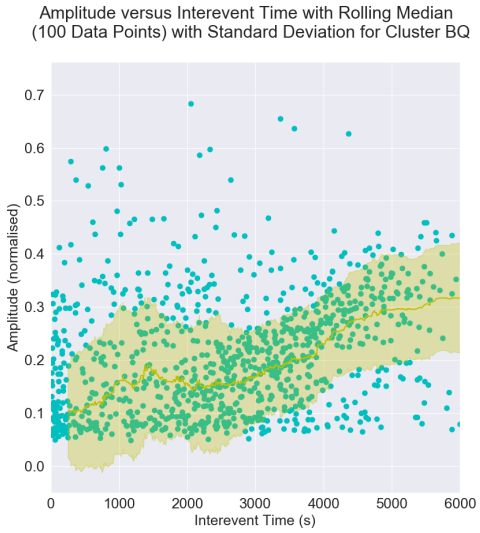

Figure 23: A rolling median fit of amplitude versus interevent time for cluster BQ for 90% of the data. Shaded bands indicate one standard deviation. It is clear that this is a possitive relation ship.

Station	Cluster BQ	Cluster XX
RA51	1815 nm/s	1646 nm/s
RA52	1194 nm/s	871 nm/s
RA53	788 nm/s	922 nm/s

Table 2: Mean vertical ground velocities of events from clusters BQ and XX per station.

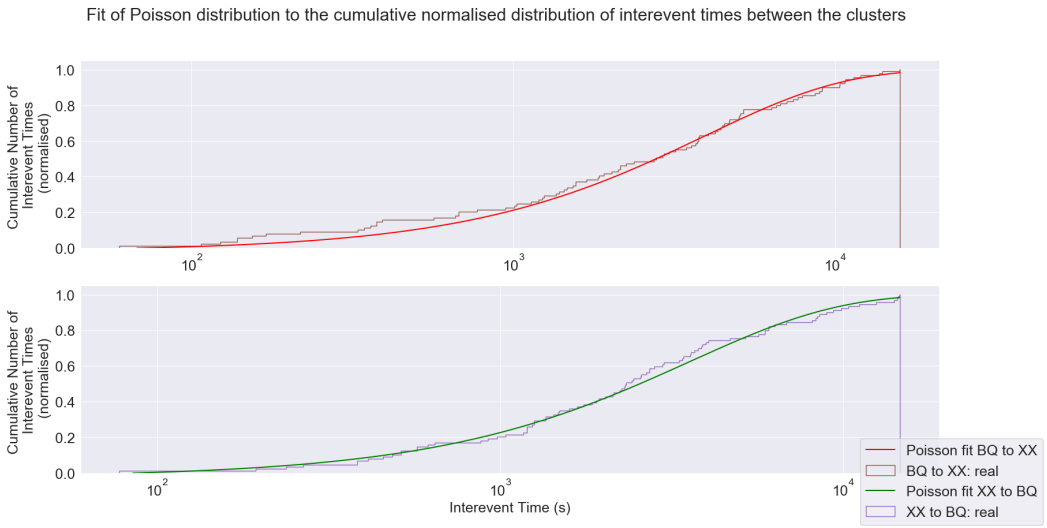

Figure 24: A fit of a Poisson distribution to cumulative distribution of the interevent times of cluster BQ to XX and cluster XX to BQ. The larger the difference between the Poisson and the cumulative histogram, the more likely it is that this difference is not random.

E Cluster Activity and Environmental Parameters through Time

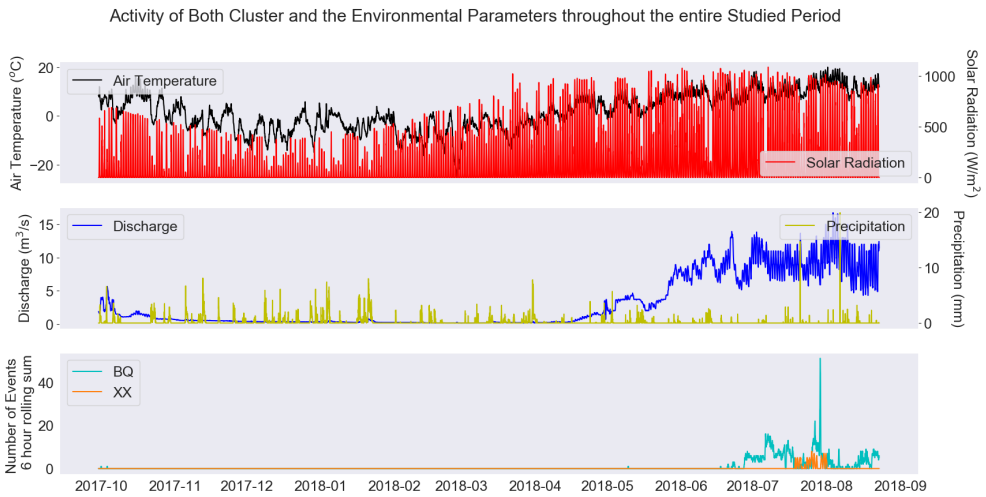

Figure 25: The relation between cluster activity of both clusters and the environmental parameters over the entire studied period. Cluster activity is a 6 hour sum, the other parameters are hourly values. It is clear that the BQ becomes only really active starting from 17-06-2018. This change is parallel to the rise in discharge, air temperature and solar radiation. Time in UTC.

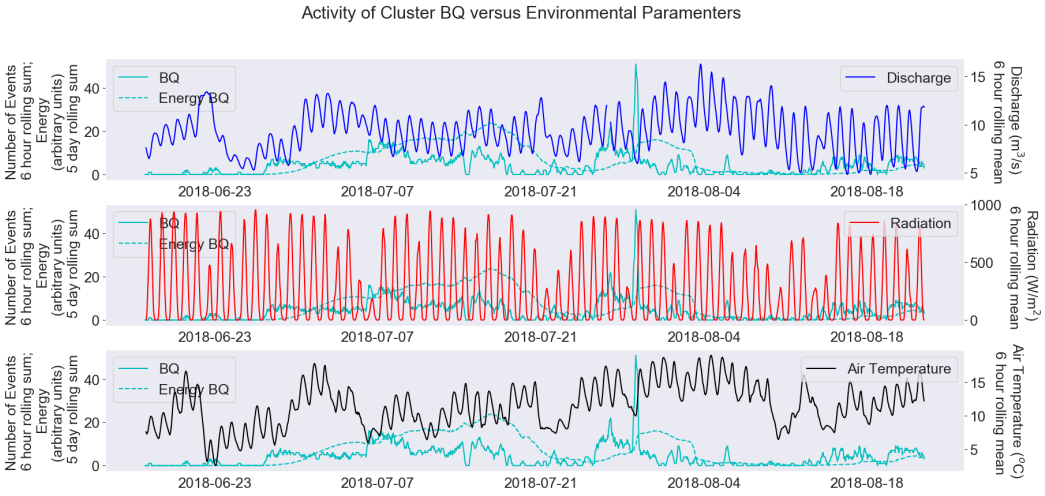

Figure 26: The relation between cluster activity of BQ and the environmental parameters over the active period. Cluster activity is a 6 hour rolling sum, energy is a 5 day rolling sum, environmental parameters are 6 hour rolling means. There does not seem to be a clear correlation between the activity and any parameters. Time in UTC.

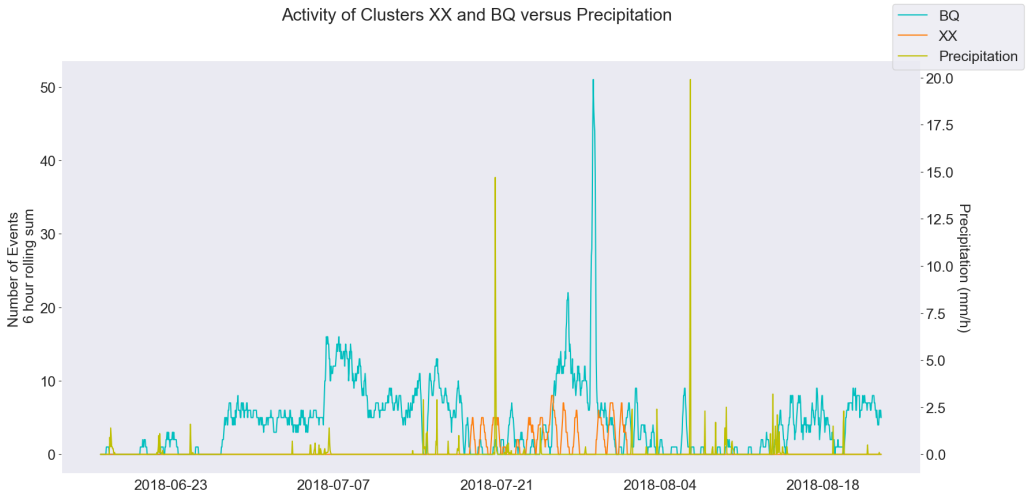

Figure 27: The relation between cluster activity of BQ and XX and precipitation over the active period. Cluster activity is a 6 hour rolling sum. Precipitation sometimes seems to precede an increase in cluster activity, but it often takes place during low activity. Time in UTC.